Aviation induced diurnal North Atlantic cirrus cover cycle

Kaspar Graf,[1] Ulrich Schumann,[1] Hermann Mannstein,[1] and Bernhard Mayer[1,2]

Received 5 June 2012; revised 20 July 2012; accepted 23 July 2012; published 29 August 2012.

[1] Aviation induced cirrus (AIC) cover is identified from mean diurnal cycles of cirrus cover and air traffic density in the North Atlantic flight corridor. Traffic data for this region show an aviation "fingerprint" with two maxima during morning eastbound and afternoon westbound traffic. The same aviation fingerprint is found in cirrus cover. Cycle differences between west and east domain parts allow separating between aviation and natural diurnal changes. Cirrus cover is derived from 8 years of Meteosat infrared data. Linear contrail cover is estimated from the same data. Background cirrus without aviation impact is estimated from cirrus observations over the South Atlantic and from numerical weather prediction forecast. The cirrus cover cycle is well approximated by linear response to traffic density with fitted delay times of 2.3–4.1 h, implying AIC cover of 1–2%, more than expected from recent models.
Citation: Graf, K., U. Schumann, H. Mannstein, and B. Mayer (2012), Aviation induced diurnal North Atlantic cirrus cover cycle, *Geophys. Res. Lett.*, *39*, L16804, doi:10.1029/2012GL052590.

1. Introduction

[2] Aircraft induce aerosol and contrails which cause aviation induced cirrus (AIC) composed of linear contrails, contrail cirrus, and possibly large-scale cirrus changes [*Fahey et al.*, 1999; *Lee et al.*, 2010]. AIC contributions were estimated from long-term trends of cirrus cover in regions of high and low air traffic density [e.g., *Stordal et al.*, 2005], however, with uncertainty in attribution of the observed changes to aviation as single cause. Because of this uncertainty, cirrus changes by aviation are treated with lower confidence than linear contrails in climate assessments [*Forster et al.*, 2007]. Models have been developed to simulate linear contrail cover [e.g., *Frömming et al.*, 2011], contrail cirrus [e.g., *Burkhardt and Kärcher*, 2011], and cirrus cover changes from aviation induced aerosols (soot etc.) [*Penner et al.*, 2009; *Hendricks et al.*, 2011]. The AIC computed can only indirectly be compared with observations because no AIC cover observations exist so far. AIC cirrus is difficult to detect in principle, and has uncertain lifetimes. Linear contrails can be detected in satellite data and have been followed for up to a day before they dissipate or mix with other contrails or cirrus [*Mannstein et al.*, 1999; *Haywood et al.*, 2009].

[3] Here we identify AIC over the North Atlantic by making use of a special diurnal traffic pattern, also found in cirrus cycles. The analysis uses cirrus cover (CC) as derived from satellite data [*Krebs et al.*, 2007; *Ewald et al.*, 2012] for the period 02/2004–01/2012. In addition we show linear contrail cover (LiCC) results. The magnitude of regional AIC cover contribution and its delay times are estimated using linear response models.

2. Methods and Data

[4] The North Atlantic region (NAR) at 45°W–10°W, 45°N–55°N includes a large part of the North Atlantic flight corridor, and is viewed by Meteosat (satellite zenith angles 53°–76°), see Figure 1. The region spans over 2500 × 1000 km^2. For comparison we consider the South Atlantic region (SAR) at 45°W–10°W, 45°S–55°S with very little air traffic. We also consider the western (W) and eastern (E) half parts of these regions.

[5] Air traffic density (ATD) data, defining flight distances per time and area were provided for the region shown in Figure 1 by the European Organization for the Safety of Air Navigation (EUROCONTROL), with 15 min time resolution and 0.25° spatial resolution, as derived from six weeks of traffic data representative for the mean ATD cycle in NAR (see auxiliary material).[1]

[6] CC is derived from data of SEVIRI (Spinning Enhanced Visible and Infrared Imager) on the geostationary Meteosat-8/9 satellites [*Schmetz et al.*, 2002] since February 2004/December 2007. For day and night cirrus detection we use the Meteosat cirrus detection algorithm MeCiDA [*Krebs et al.*, 2007] in its improved version MeCiDA2 [*Ewald et al.*, 2012]. MeCiDA2 combines morphological and multi-spectral threshold tests and detects ice clouds making use of 7 infrared (IR) channels at 6.2, 7.3, 8.7, 9.7, 10.8, 12.0, and 13.4 μm. The detection efficiency exceeds 50% for cirrus optical depth (550 *nm*) above about 0.1–0.25 [*Krebs et al.*, 2007]. MeCiDA2 provides a binary cirrus mask (0 or 1) at the Meteosat resolution of about 5 km every 15 min, see Figure 1 (middle). Temporal gaps (1.6% of all time steps, e.g., due to missing data) are linearly interpolated in time.

[7] The initially linear shape of contrails is used by the contrail detection algorithm (CDA) [*Mannstein et al.*, 1999] to derive the LiCC from IR brightness temperature data at the same resolution as MeCiDA2. The algorithm has been used before to derive LiCC from polar orbiting multi-channel images [e.g., *Palikonda et al.*, 2005]. The algorithm is applicable to Meteosat data, though with lower detection efficiency (10%) and higher false alarm rate (1.2%), because of the lower spatial resolution of SEVIRI compared to polar satellite sensors [*Mannstein et al.*, 2010].

[8] As one approximation for cirrus without aviation we consider medium-range numerical weather prediction of high cloud cover (HCC) by the European Centre for Medium-Range Weather Forecasts (ECMWF). Aviation effects are

[1]Institut für Physik der Atmosphäre, Deutsches Zentrum für Luft- und Raumfahrt, Oberpfaffenhofen, Germany.
[2]Meteorologisches Institut München, Ludwig-Maximilian-Universität München, Munich, Germany.

Corresponding author: K. Graf, Institut für Physik der Atmosphäre, Deutsches Zentrum für Luft- und Raumfahrt, Postfach 1116, D-82234 Oberpfaffenhofen, Germany. (kaspar.graf@dlr.de)

0094-8276/12/2012GL052590

[1]Auxiliary materials are available in the HTML. doi:10.1029/2012GL052590.

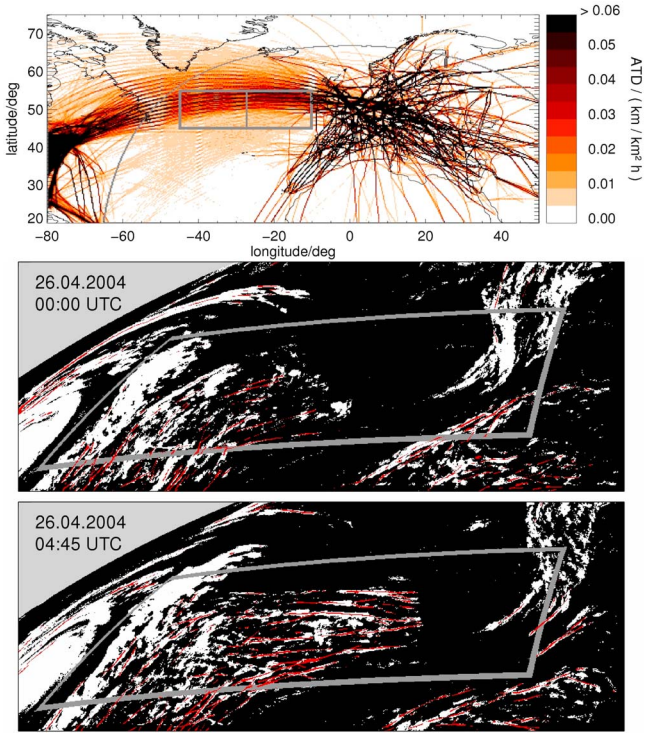

Figure 1. (top) Mean air traffic density. The grey box indicates the NAR location and its western and eastern parts. MeCiDA2 results for 26 April 2004 (middle) 00:00 UTC, and (bottom) 04:45 UTC, in original Meteosat grid. The grey box indicates the NAR. Red pixel indicate linear cirrus structures detected by the CDA. Animated ATD and MeCiDA2 scenes are in the auxiliary material.

not included in this model but may impact initial values. Hence, after some time the initial disturbances decay, and any remaining diurnal cycles in HCC forecast reflect natural variability. Here we analyze the diurnal cycle of HCC for the year 2011. ECMWF provides forecasts every 3 h up to 144 h with 0.25° horizontal resolution. To reduce spin-up effects, we use data from the medium-range forecast period 96–144 h (4–6 d), average over forecasts from 00 UTC and 12 UTC analyses, and subtract small remaining linear HCC trends, see Figure 2.

[9] Area mean cover $c(t_i, d, y)$ is computed for NAR and SAR and their subregions W and E by averaging over all pixels, weighted with pixel sizes, for years $y = 1, \ldots, Y = 8$, days $d = 1, \ldots, D = 364$, and universal day times $t_i = (i - 1) \cdot \Delta t$, $\Delta t = 15$ min, $i = 1, 2, \ldots, I = 96$ from the 2912 days between 1 February 2004 and 21 January 2012. This allows for 8 equal-sized subsamples or smaller samples taking every second or fourth day. In total, the data set includes 279552 time steps derived from 118329 spatial pixels for each NAR/SAR Meteosat scene.

[10] For each year y (or subsample), we compute mean diurnal cycles $C(t_i,y) = \langle c(t_i,d,y)\rangle_d - \left[\langle c(t_i,d,y)\rangle_{t_i,d} - \langle c(t_i,d,y)\rangle_{t_i,d,y}\right]$. Here, angular brackets with index define the mean value with respect to the indexed variable. The subtraction of the term in brackets […] leaves the shape of the diurnal cycle unchanged but eliminates interannual variability. For illustration see the auxiliary material. The results $C(t_i, y)$ are shown in Figure 3 (top).

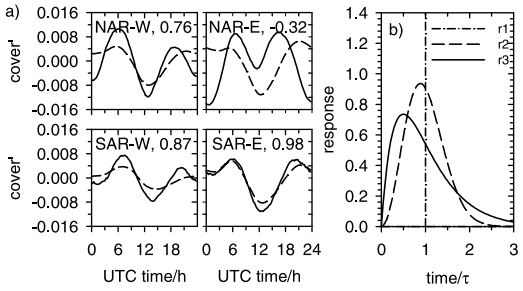

Figure 2. (a) Mean diurnal cycles of cirrus cover from MeCiDA2-CC (8 years) and ECMWF-HCC (2011) for NAR and SAR, separately for the W and E parts. Mean cover values have been subtracted. The correlation coefficients ρ between CC and HCC are given for each subregion. (b) Normalized response functions $\tau r_i(t/\tau)$, for $i = 1, 2, 3$.

[11] A linear response model is used to estimate timescale and cover of AIC. A simple model $C_m(t_i)$ is matched to the data to separate natural cirrus and AIC. The model assumes $C_m(t_i)$ to be the sum of non-aviation cirrus diurnal cycle $B(t_i)$ and AIC cover contribution $C_A(t_i)$. The non-aviation part is split into a constant mean background and its diurnal deviation, $B(t_i) = B + b(t_i)$. The AIC contribution is assumed to be proportional to air traffic density $a(t_i)$ in the past

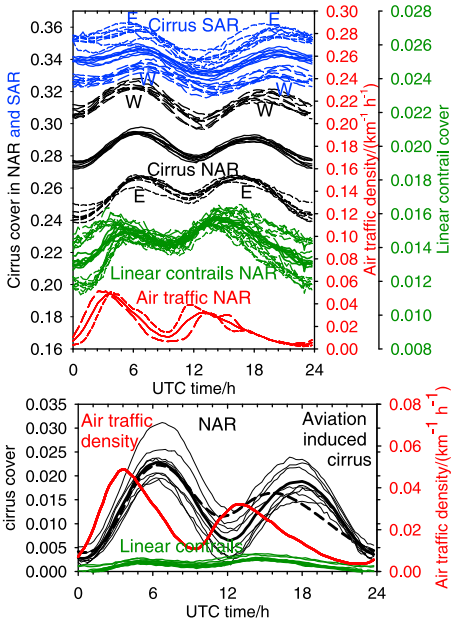

Figure 3. (top) Annual-mean diurnal cycle of air traffic density ATD (red), eight annual-mean diurnal cycles $C(t_i, y)$ of linear contrail cover LiCC (green), and cirrus cover CC in NAR (black solid), NAR-W/E (black dashed and labeled), SAR (blue solid), SAR-W/E (blue dashed and labeled). (bottom) Left axis: Annual (thin lines) and eight-year-mean (thick full line) observed CC (black), AIC (thick dashed), and mean LiCC (thin and thick green), above fitted constant backgrounds, as derived for the response function r_3, for NAR. Right axis: ATD (red line).

Table 1. Fit Results for CC and LiCC for Various Background $b(t_i)$ (Equation (3)), and Response Functions r_i, i = 1, 2, 3 (Equation (2)), Response Time τ and Its Standard Deviation $\sigma(\tau)$ in h, AIC (Equation (1)) and Its Standard Deviation σ(AIC) in Area Percentage, Pearson's Correlation Coefficient ρ, and the rms Error χ in Area Percentage

Field	$b(t_i)$	i	$\tau \pm \sigma(\tau)$	AIC $\pm \sigma$(AIC)	ρ	χ
CC	0	1	2.79 ± 0.24	0.910 ± 0.208	0.899	0.262
	0	2	2.88 ± 0.20	1.119 ± 0.264	0.904	0.256
	0	3	3.33 ± 0.98	1.407 ± 0.332	0.873	0.292
	SAR	1	2.31 ± 0.46	0.783 ± 0.350	0.871	0.344
	SAR	2	2.77 ± 1.05	1.027 ± 0.548	0.904	0.289
	SAR	3	3.62 ± 1.43	1.543 ± 0.888	0.932	0.237
	HCC	1	2.80 ± 0.26	0.921 ± 0.390	0.848	0.364
	HCC	2	3.16 ± 0.40	1.222 ± 0.556	0.892	0.301
	HCC	3	4.08 ± 0.83	1.846 ± 0.845	0.933	0.223
LiCC	0	1	1.42 ± 0.42	0.099 ± 0.045	0.774	0.048
	0	2	1.55 ± 0.50	0.108 ± 0.053	0.791	0.047
	0	3	2.39 ± 1.72	0.146 ± 0.079	0.850	0.041

according to a response function $r(t_i)$ with adjustable amplitude A and time scale τ,

$$C_m(t_i) = B + b(t_i) + C_A(t_i), \quad \text{with} \quad C_A(t_i) = A\int_{-\infty}^{t_i} a(\hat{t})r(t-\hat{t})d\hat{t}. \tag{1}$$

We use either of the following response functions r,

$$\begin{aligned} r_1(t) &= \delta(t-\tau), \\ r_2(t) &= (32/(\pi^2\tau))(t/\tau)^2 \exp\left(-(4/\pi)(t/\tau)^2\right), \\ r_3(t) &= (4t/\tau^2)\exp(-2t/\tau). \end{aligned} \tag{2}$$

The functions define the cover response to a δ-pulse traffic forcing. They are specified such that $\int_0^\infty r(t)dt = 1$, and $\tau = \int_0^\infty tr(t)dt$ is the mean delay time represented by $r(t)$. The spectrum of timescales is measured by variances $v^2 = \int_0^\infty (t-\tau)^2 r(t)dt$, v^2/τ^2 = 0, 0.178, 0.5 for the three response functions, respectively. The delta function represents just one time scale. An increase with t at small times, as in r_2 and r_3, is expected because young contrails are narrow and it takes some time until they become visible in Meteosat pixels [*Mannstein and Schumann*, 2005].

[12] For the deviation $b(t_i)$ of the non-aviation CC from its mean value, we assume either of three alternatives:

$$b(t_i) = 0, \; b(t_i) = \langle C_{\mathrm{SAR}}(t_i, y)\rangle_y, \; b(t_i) = C_{\mathrm{HCC}}(t_i). \tag{3}$$

The 1st alternative assumes a constant mean cycle of non-aviation cirrus. The 2nd assumes the non-aviation deviation part in the NAR to be as observed in the SAR. The 3rd assumes that it equals the HCC forecast for the NAR. The three fit parameters B, A, and τ are determined by minimizing the root-mean square (rms) error χ, $\chi^2(y) = \left\langle (C(t_i,y) - C_m(t_i))^2 \right\rangle_{t_i}$. We report fit results for $C(t_i, y)$ being either CC or LiCC in either the total NAR or the E or W half-domains. For the LiCC case, a constant false alarm rate is assumed ($b(t_i) = 0$). For assessing both, the fit results and their interannual variability, the fit is computed separately for each of the (annual) samples giving Y different fit results $B(y)$, $A(y)$, $\tau(y)$. These values allow for computation of the day mean AIC cover $\langle C_A(t_i, y)\rangle_{t_i}$ and mean values of $\tau(y)$, their standard deviations σ and the Pearson's correlation coefficients ρ between $C(t_i, y)$ and $C_m(t_i)$, see Table 1.

3. Results

3.1. Satellite Observed Cirrus Cover Distribution

[13] MeCiDA2 cirrus cover scenes show AIC formation in the NAR. This is obvious in particular in animations of high spatial resolution scenes every 15 min, see auxiliary material. Figure 1 (middle) shows two representative examples. One finds increases in CC shortly after passage of traffic in regions with high ATD. Most obvious are linear clouds indicating contrails, partially forming in cloudfree regions. These clouds are typically several km wide and sometimes hundreds of km long. The animations show clusters of contrails forming after traffic passage in suitable meteorological conditions which occur about every 3rd day, often over several days. The clusters have lifetimes of order hours.

[14] However, this paper does not intend to identify AIC only from cloud structures. In fact, by far not all AIC clouds are visible as linear clouds. Some AIC just fill cloud gaps or extend cloudiness at the edges of preexisting cirrus. Such changes cannot be identified as AIC by an observer without additional means.

3.2. Air Traffic Density Diurnal Cycle

[15] As shown in Figure 3 (top), the diurnal cycle of air traffic in the NAR follows a special pattern: The majority of the eastbound traffic leaves North America in the evening and arrives in Europe in the morning (local time). The majority of the westbound traffic leaves Europe in the late morning arriving in North America in the afternoon. Consequently, the mean diurnal cycle of ATD has a distinctive pattern characterized by two traffic peaks in NAR – the eastbound centered at 03:45 UTC and the westbound centered at 13:00 UTC. The maximum (minimum) ATD averaged over the whole North Atlantic region, 0.05 (0.0037) $\mathrm{km}^{-1}\,\mathrm{h}^{-1}$ occurring at 03:45 (22:45) UTC is 2.3 times larger (5.5 times smaller) than the 24 h mean ATD of 0.021 $\mathrm{km}^{-1}\,\mathrm{h}^{-1}$. The morning and afternoon parts of the ATD cycle differ in that the eastbound morning traffic occurs in a rather narrow time period and often follows the great circle routes through the NAR, while the westbound traffic spreads over a larger time period and often deviates further north to avoid strong headwinds. ATD in the western and eastern parts exhibit significantly different cycle patterns: In the morning, eastbound traffic peaks first in the W and about 1–1.5 h later in the E because of 1250 km separation and about 900 km h^{-1} aircraft speed with tail winds. In the afternoon, the sequence is the opposite: traffic peaks around 11:30 UTC first in E and, because of head winds, about 1.5–2 h later in W (see Animation S1 and Table S2).

3.3. Linear Clouds and Cirrus Cover Diurnal Cycles

[16] The diurnal cycle of NAR CC (see Figure 3, top) exhibits various characteristic features similar to those of ATD. CC has two maxima, the first occurring at 06:28 UTC ± 00:16 and a second about 11 h later at 17:45 UTC ± 00:24, and two

minima at 12:10 UTC ± 00:15 and 0:08 UTC ± 00:20. The two cirrus peaks appear to be related to the rush hours of air traffic. The CC follows the ATD signal with about 3–5 h delay, a reasonable time for forming and decaying detectable contrail cirrus. As for ATD, the cirrus cycle peaks are further separated in time in W and closer together in E. As westbound flights first arrive in W and eastbound flights first arrive in E, the cirrus cycles are fully consistent with the ATD fingerprint. The pattern on NAR is significantly different from the pattern in SAR. This fingerprint is conserved in cover differences NAR-SAR of MeCiDA2 results (see auxiliary material) and in differences of MeCiDA2-NAR cover and ECMWF-NAR HCC.

[17] However, also the SAR diurnal cycle of CC exhibits a double wave. The SAR-W and SAR-E cirrus cycles show patterns which are shifted according to local time, see Figure 2. The sun rises first in the eastern part and 1.2 h later in the western part and causes migrating solar tides [*Hagan and Forbes*, 2002] (see auxiliary material). Also the semi-diurnal CC maxima in SAR migrate with daytime. They are apparently represented in the ECMWF model HCC results. The correlation between MeCiDA2 and HCC is higher in SAR than in NAR, see Figure 2. This further supports the assumption that the CC SAR observations and the HCC NAR forecasts approximate the natural diurnal cycle, and the cover on top of this background is the AIC signal.

3.4. Aviation Induced Cloud Changes From Model Fits

[18] Fits were computed for the various response models and background assumptions defined above for each individual year. The fit mean values and their standard deviations are given in Table 1. The computed AIC percentage cover is positive. The fit results are more sensitive to the selected response functions than to the different non-aviation deviations $b(t_i)$ (equation (3)). The responses show reasonable correlation coefficients >0.8, approximation errors of about 0.3 for percentage cover and 0.5 h for the timescales, comparable to the standard deviations characterizing interannual variability, for all parameter combinations. The timescales are within 2.3–4.1 h for AIC and 1.4–2.4 h for LiCC. The LiCC cover is estimated between 0.1–0.15% cover. Larger timescales and larger cover for AIC than LiCC were to be expected. The AIC cover in NAR amounts to 0.9–1.9%. Smallest AIC is computed for narrow response (Dirac delta function). A significant AIC doublewave is computed only for timescales smaller than the 9.5 h separation between the two NAR traffic peaks. SAR background gives the smallest and ECMWF HCC forecast the largest AIC contribution. Constant background with response function r_3 give slightly smaller fit errors, higher correlations, and shows similar interannual and fit uncertainties. Figure 3 (bottom) illustrates the ATD and the LiCC and AIC responses, with increasing delay times.

4. Discussions

[19] The observed CC and the delayed response to ATD do not correlate perfectly (Figure 3, bottom). The observed CC amounts are about equal in the morning and afternoon while the mean morning ATD signal is larger than in the afternoon. The observed CC peaks 5 h after the ATD peak in the afternoon but 3 h later in the morning. The observed LiCC first increases with ATD but suddenly decreases when ATD peaks. Perfect correlations were not to be expected because the response model does not account for contrail advection, nonlinear contrail response to ATD, diurnal variations in meteorology, saturation in LiCC detection, etc.

[20] Also, MeCiDA2 might cause some of the differences. MeCiDA2 uses six individual cirrus tests of different SEVIRI channel combinations. The diurnal CC cycle determined applying each test alone is consistent with the total MeCiDA2 result (not shown). Hence, diurnal-cycle artifacts from, e.g., the 9.7-μm ozone channel, are excluded. Averaging separately over data from Meteosat 8 and 9, with slightly different SEVIRI properties and satellite positions, or using MeCiDA results instead of MeCiDA2, does not change the results significantly. Selecting even and odd days separately for 16 instead of 8 annual samples gives the same means and similar standard deviations. For 32 samples, the standard deviations exceed the mean values.

[21] The derived AIC cover of 1–2% in NAR is about 10 times larger than the detected LiCC (0.1–0.15%). A factor ten was estimated before over Europe [*Mannstein and Schumann*, 2005]. The high ratio may reflect the low CDA detection efficiency. The observed AIC cover in NAR is larger and has higher optical depth τ_s (MeCiDA2 threshold $\tau_s > 0.1$) than previously computed (0.5% for line-shaped contrails [*Frömming et al.*, 2011], 1% for contrail cirrus [*Burkhardt and Kärcher*, 2011], both for NAR with $\tau_s > 0.02$). Hence, our results imply a larger climate effect. The derived delay time is shorter than the lifetimes found in a recent model study [*Newinger and Burkhardt*, 2012]. Though the lifetime is not the same as the delay time, longer timescales tend to smear out the double wave.

5. Conclusions

[22] The observations and model results show that aviation induces observable changes in cirrus cover over the North Atlantic. The cirrus cover derived from day and night Meteosat data show on average for all 8 years, as well as for individual years, a specific pattern. The mean cycle is characterized by a double wave which follows the mean diurnal cycle of air traffic with a delay time of about 3–5 h. Constant background or background as observed in SAR or as modelled in medium range ECMWF forecasts for NAR give similar results. The observed NAR cirrus cycle correlates well with ATD, also separately in the west and east parts of the NAR, while the also existing cirrus double-waves in the South Atlantic are caused by the variation of solar radiation due to Earth rotation. The cirrus cycle amplitude is positive and larger than that of linear contrails derived from the same Meteosat data, and the LiCC signal peaks in time between the ATD and CC maxima.

[23] The NAR cirrus patterns are well approximated by linear response functions with fitted delay times of 2.3–4.1 h, and AIC amounts to 1 to 2%, regardless of which of the three assumptions on cirrus without aviation is taken. These amplitudes are large enough to be significant in spite of large cirrus variability. Smallest AIC values correspond to the narrowest response function. The time spectrum represented by the response functions cannot be arbitrarily wide because the fits get smoothed for wide time spectra and no longer represent the two maxima in the observations. Hence, the given range of AIC values may embrace the true aviation contribution to the diurnal cycle.

[24] AIC contributions at timescales ≥1 d do not contribute to the diurnal cirrus cycle and hence cannot be detected at these time and space scales. Future studies may investigate whether the ATD signals become visible in longer cirrus cycles and larger domains. As the observational fingerprint is restricted to the NAR discussed in this paper, models are needed to extrapolate the regional results to the globe. The observations presented in this paper can be used for contrail cirrus model validation.

[25] **Acknowledgments.** We thank S. Rentsch for data handling support. Meteosat 8/9 data were provided by Eumetsat via the German Remote Sensing data center at DLR, and air traffic data were provided by Eurocontrol, both within the ESA-DUE project "contrails". The work performed was part of the DLR projects PAZI 2 and CATS, and the BMBF project UFO within Klimazwei framework. ECMWF data were provided within the ECMWF special project SPDERIMS.

[26] The Editor thanks the two anonymous reviewers for assisting in the evaluation of this paper.

References

Burkhardt, U., and B. Kärcher (2011), Global radiative forcing from contrail cirrus, *Nat. Clim. Change*, *1*, 54–58, doi:10.1038/nclimate1068.

Ewald, F., L. Bugliaro, H. Mannstein, and B. Mayer (2012), An improved cirrus detection algorithm MeCiDA2 for SEVIRI and its validation with MODIS, *Atmos. Meas. Tech. Discuss.*, *5*, 5271–5311, doi:10.5194/amtd-5-5271-2012.

Fahey, D., et al. (1999), Aviation-produced aerosols and cloudiness, in *Aviation and the Global Atmosphere. A Special Report of Working Groups I and III of the Intergovernmental Panel on Climate Change*, edited by J. E. Penner et al., pp. 65–120, Cambridge Univ. Press, New York.

Forster, P., et al. (2007), Changes in atmospheric constituents and in radiative forcing, in *Climate Change 2007: The Physical Science Basis. Contribution of Working Group I to the Fourth Assessment Report of the Intergovernmental Panel on Climate Change*, edited by S. Solomon et al., pp. 129–234, Cambridge Univ. Press, New York.

Frömming, C., M. Ponater, U. Burkhardt, A. Stenke, and R. Sausen (2011), Sensitivity of contrail coverage and contrail radiative forcing to selected key parameters, *Atmos. Environ.*, *45*, 1483–1490, doi:10.1016/j.atmosenv.2010.11.033.

Hagan, M. E., and J. M. Forbes (2002), Migrating and nonmigrating diurnal tides in the middle and upper atmosphere excited by tropospheric latent heat release, *J. Geophys. Res.*, *107*(D24), 4754, doi:10.1029/2001JD001236.

Haywood, J. M., R. P. Allan, J. Bornemann, P. M. Forster, P. N. Francis, S. Milton, G. Rädel, A. Rap, K. P. Shine, and R. Thorpe (2009), A case study of the radiative forcing of persistent contrails evolving into contrail-induced cirrus, *J. Geophys. Res.*, *114*, D24201, doi:10.1029/2009JD012650.

Hendricks, J., B. Kärcher, and U. Lohmann (2011), Effects of ice nuclei on cirrus clouds in a global climate model, *J. Geophys. Res.*, *116*, D18206, doi:10.1029/2010JD015302.

Krebs, W., H. Mannstein, L. Bugliaro, and B. Mayer (2007), Technical note: A new day- and night-time Meteosat Second Generation Cirrus Detection Algorithm MeCiDA, *Atmos. Chem. Phys.*, *7*(24), 6145–6159, doi:10.5194/acp-7-6145-2007.

Lee, D. S., et al. (2010), Transport impacts on atmosphere and climate: Aviation, *Atmos. Environ.*, *44*(37), 4678–4734, doi:10.1016/j.atmosenv.2009.06.005.

Mannstein, H., and U. Schumann (2005), Aircraft induced contrail cirrus over Europe, *Meteorol. Z.*, *14*(4), 549–554, doi:10.1127/0941-2948/2005/0058.

Mannstein, H., R. Meyer, and P. Wendling (1999), Operational detection of contrails from NOAA-AVHRR data, *Int. J. Remote Sens.*, *20*, 1641–1660, doi:10.1080/014311699212650.

Mannstein, H., A. Brömser, and L. Bugliaro (2010), Ground-based observations for the validation of contrails and cirrus detection in satellite imagery, *Atmos. Meas. Tech.*, *3*(3), 655–669, doi:10.5194/amt-3-655-2010.

Newinger, C., and U. Burkhardt (2012), Sensitivity of contrail cirrus radiative forcing to air traffic scheduling, *J. Geophys. Res.*, *117*, D10205, doi:10.1029/2011JD016736.

Palikonda, R., P. Minnis, D. P. Duda, and H. Mannstein (2005), Contrail coverage derived from 2001 AVHRR data over the continental United States of America and surrounding areas, *Meteorol. Z.*, *14*, 525–536, doi:10.1127/0941-2948/2005/0051.

Penner, J. E., Y. Chen, M. Wang, and X. Liu (2009), Possible influence of anthropogenic aerosols on cirrus clouds and anthropogenic forcing, *Atmos. Chem. Phys.*, *9*(3), 879–896, doi:10.5194/acp-9-879-2009.

Schmetz, J., P. Pili, S. Tjemkes, D. Just, J. Kerkmann, S. Rota, and A. Ratier (2002), An introduction to Meteosat Second Generation (MSG), *Bull. Am. Meteorol. Soc.*, *83*, 977–992.

Stordal, F., G. Myhre, E. J. G. Stordal, W. B. Rossow, D. S. Lee, D. W. Arlander, and T. Svendby (2005), Is there a trend in cirrus cloud cover due to aircraft traffic?, *Atmos. Chem. Phys.*, *5*(8), 2155–2162, doi:10.5194/acp-5-2155-2005.